analytical chemistry

Article

pubs.acs.org/ac

Single-Shot Characterization of Enzymatic Reaction Constants K_m and k_{cat} by an Acoustic-Driven, Bubble-Based Fast Micromixer

Yuliang Xie,[†,‡] Daniel Ahmed,[‡] Michael Ian Lapsley,[‡] Sz-Chin Steven Lin,[‡] Ahmad Ahsan Nawaz,[‡] Lin Wang,[§] and Tony Jun Huang*[,†,‡]

[†]Department of Chemical Engineering, The Pennsylvania State University, University Park, Pennsylvania 16802, United States

[‡]Department of Engineering Science and Mechanics, The Pennsylvania State University, University Park, Pennsylvania 16802, United States

[§]Ascent Bio-Nano Technologies Inc., State College, Pennsylvania 16801, United States

Supporting Information

ABSTRACT: In this work we present an acoustofluidic approach for rapid, single-shot characterization of enzymatic reaction constants K_m and k_{cat}. The acoustofluidic design involves a bubble anchored in a horseshoe structure which can be stimulated by a piezoelectric transducer to generate vortices in the fluid. The enzyme and substrate can thus be mixed rapidly, within 100 ms, by the vortices to yield the product. Enzymatic reaction constants K_m and k_{cat} can then be obtained from the reaction rate curves for different concentrations of substrate while holding the enzyme concentration constant. We studied the enzymatic reaction for β-galactosidase and its substrate (resorufin-β-D-galactopyranoside) and found K_m and k_{cat} to be 333 ± 130 μM and 64 ± 8 s^{-1}, respectively, which are in agreement with published data. Our approach is valuable for studying the kinetics of high-speed enzymatic reactions and other chemical reactions.

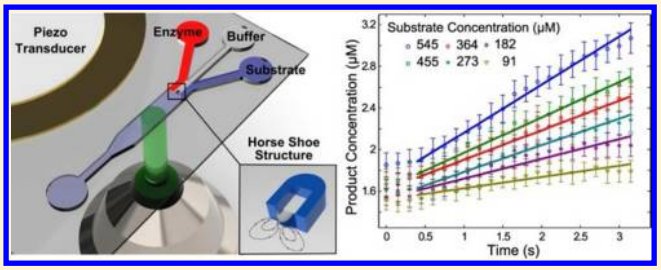

Enzymes have played an important role in many disciplines such as biochemistry,[1,2] medicine,[3,4] food science,[5,6] and biochemical engineering.[7,8] One key issue in enzyme-based assays and studies is the accurate characterization of the enzymatic reaction constants.[9−11] The Michaelis−Menten (M−M) kinetics is one of the most used models to describe the bulk reactions of enzymes,[12,13] and the M−M constant (K_m) and turnover number (k_{cat}) are two of the most important constants in enzymatic reactions. K_m quantifies the affinity between enzyme and substrate; k_{cat} quantifies the turnover rate of the reaction. A typical strategy used to calculate K_m and k_{cat} is the Lineweaver−Burk plot (L−B plot).[14] This method uses a linear regression of the reciprocal of both the initial reaction rate (v_0) and the substrate concentration (C_0) from the M−M kinetics equation to calculate the enzymatic reaction constants.

Microfluidics[15] has emerged as a powerful platform for chemical,[16−18] biological,[19−22] and physical[23−27] processes due to its simple fabrication, ultralow sample consumption, and ease of use. Using a microfluidic device to measure the enzymatic reaction constants requires two key factors: first, several parallel experiments must be conducted with different substrate concentrations but a constant enzyme concentration and second, enzyme and substrate must be mixed as quickly as possible to quantify the initial reaction and minimize the time that substrate or enzyme is inhomogeneous due to partial mixing. Following these two requirements, several microfluidic-based approaches have been developed to measure enzymatic reaction constants.[28−42] These approaches can potentially examine many enzymatic reactions in parallel while consuming smaller amounts of samples and reagents than conventional methods. In these approaches, however, the kinetics of high-speed enzymatic reactions is often difficult to characterize because the mixing is slow. The mixing time is on the order of 10 s if the mixing is driven by diffusion.[30,31,35,37] The mixing time is about 1 s when convection, such as Dean flow, is introduced.[29,38] The relatively long mixing time makes these approaches only applicable to enzymatic reactions with long reaction times, in these reactions the reaction time has to be significantly longer than the mixing time. Thus, there is a strong need for developing rapid microfluidic mixers for accurate on-chip characterization of high-speed enzymatic reactions. In this regard, the Ismagilov group and other researchers have successfully measured the enzymatic reaction constants using multiphase flow with induced vortex mixing within a droplet to rapidly mix the enzyme and substrate.[33,34,39−42] This approach successfully improved mixing efficiency in droplets; however, it introduced an organic solvent that may increase the complexity of experiments and/or change the properties of the reaction kinetics due to the interfacial effects. It would be advantageous to have a system that induces fast mixing without the use of organic solvents.

Received: June 9, 2012
Accepted: July 29, 2012
Published: July 29, 2012

   dx.doi.org/10.1021/ac301590y | *Anal. Chem.* 2012, 84, 7495−7501

Acoustofluidic micromixers can effectively enhance mixing efficiency without the use of organic solvents. In our previous work, an acoustic-driven bubble leads to ultrafast mixing in a microfluidic channel.[43,44] When a bubble is introduced in the microfluidic channel and driven by acoustic waves, the oscillating gas–liquid interface will cause vortices in the channel to achieve millisecond level mixing. This method is well suited for use in measuring enzymatic reaction constants.

In this article, we report an on-chip, single-shot characterization system that uses an acoustic bubble-based microfluidic mixer to measure the enzymatic reaction constants. "Single-shot" means the concentration of enzyme and substrate are adjusted by altering the flow rates of the pumps during a single experiment. Our "single-shot" method allows streamlining of the experiments to save time in parallel experiments and ensures that all experimental parameters are consistent. The enzyme and substrate were fully mixed in just a few milliseconds by the oscillating bubble. The fast enzymatic reaction between β-galactosidase (β-Gal) and its substrate, resorufin β-D-galactopyranoside, was tested using this system. This reaction led to a fluorescent product to facilitate the detection. The intensity of the fluorescent signals indicated the concentration of product generated from the reaction. The reaction time was calculated based on the flow rates and the geometry of the channel. Our bubble-based, high-speed mixer reduced the mixing time into the milliseconds range, significantly increasing the versatility in characterizing enzymatic reaction constants without the use of organic solvents or measures to affect the reaction. In addition, our continuous flow design can record all the information in the initial phase of the enzymatic reaction with high resolution, which has advantages over conventional methods that can only record separated data points.

EXPERIMENTS

Device Fabrication. The polydimethylsiloxane (PDMS) based microfluidic channel was fabricated using the standard soft lithography and mold replica technique.[45] The channel design is shown in Figure 1. The channel width, depth, and length are 570 μm, 65 μm, and 1.5 cm, respectively. A horseshoe structure is positioned at the center of the channel to trap a bubble inside (insert in Figure 1). The width, depth, and length for the horseshoe structure are 60 μm, 65 μm, and 90 μm, respectively. The PDMS channel was treated with oxygen plasma and bonded to a glass slide. The bubble was trapped inside the horseshoe structure by injecting reaction buffer from the outlet of the channel. A piezoelectric transducer (model no. 273-073, RadioShack Corp.) was bonded adjacent to the PDMS microfluidic device on the same glass substrate using epoxy. The piezoelectric transducer was driven by a function generator (Hewlett-Packard 8116A) using a square wave with a frequency equal to the natural resonance frequency (31 kHz) of the trapped bubble.

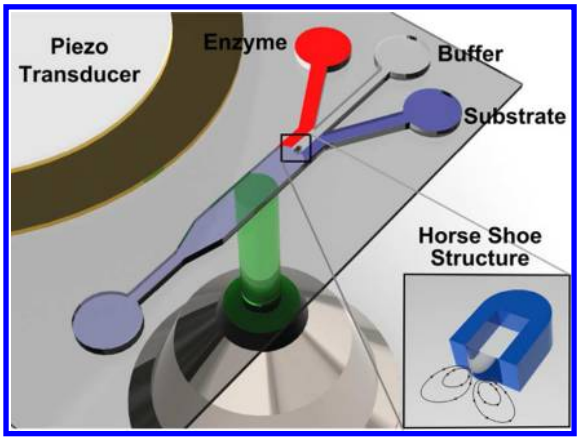

Figure 1. Schematic of the experimental setup. The inset shows the horseshoe structure with a bubble trapped inside.

On-Chip Enzymatic Reaction. In our experiments, the enzyme characterized was β-galactosidase (from *Escherichia coli*). The reaction buffer contains 100 mM Tris, 2.0 mM KCl, 0.1 mM $MgCl_2$, 0.1% BSA (w/w), and 0.05% Tween 20 (w/w) at pH 7.8. The enzyme was dissolved in reaction buffer to form the enzyme solution. The substrate, resorufin-β-D-galactopyranoside, was stored in dimethyl sulfoxide at −20 °C. The chemicals above were purchased from Sigma-Aldrich. Immediately before use, the thawed stock solution was diluted with the reaction buffer to form substrate solution. The enzyme solution, reaction buffer, and substrate solution were injected into the reaction channel with syringe pumps (KD Scientific Corp.). The reaction buffer was injected in the middle inlet to separate the enzyme and substrate and to prevent reaction before mixing (Figure 1). The standard material of reaction product, sodium resorufin, was used to correlate the fluorescent intensity with the concentration of the product. All experiments were carried out at room temperature.

Optical Detection Setup. While the enzyme and substrate do not emit fluorescence, the enzymatic reaction is a fluorescence-generating reaction. The reaction product, resorufin, has a maximum emitting fluorescent intensity at 585 nm, while the maximum exciting wavelength is 570 nm. A fluorescent intensity detection system was constructed to monitor the change in product concentration. A transmission microscope (Elipse Ti, Nikon Corp.), combined with two bandpass filters (530–570 nm and 580–650 nm, respectively) and one dichroic mirror (transmission above 575 nm), was used to observe the fluorescent light. A CCD camera (CoolSNAP HQ2, Photometrics) was connected to the microscope for capturing images. The parameters used in the optical setup were held fixed over all the experiments.

RESULTS AND DISCUSSION

Fast Mixing. The gas–liquid interface oscillates when the bubble is stimulated by the acoustic waves from the piezoelectric transducer. This oscillation has a maximum amplitude at the fundamental resonance frequency of the bubble, which depends on the size of the bubble and the properties of the liquid. For a water-based reaction environment, a bubble, with dimensions of 60 μm (width) × 90 μm (length) × 65 μm (height), has a resonance frequency at ∼31 kHz. Under these conditions, the bubble will get stable oscillation and can maintain its shape for more than 10 min. The bubble's oscillatory frequency was the same as that of the stimulating signal, and its oscillation amplitude was approximately 5 μm. The oscillating bubble changed the flow field near its surface and caused fast mixing in the fluid. To visualize and characterize the rapid mixing in our bubble-based mixer, blue, clear, and red fluids are shown to represent the substrate, buffer, and enzyme, respectively, we used in the experiment (Figure 2a). The flow rates of the three fluids were set as 0.4, 0.3, 0.4 μL/min, which were the same as in our enzymatic reaction experiments. When the piezoelectric transducer

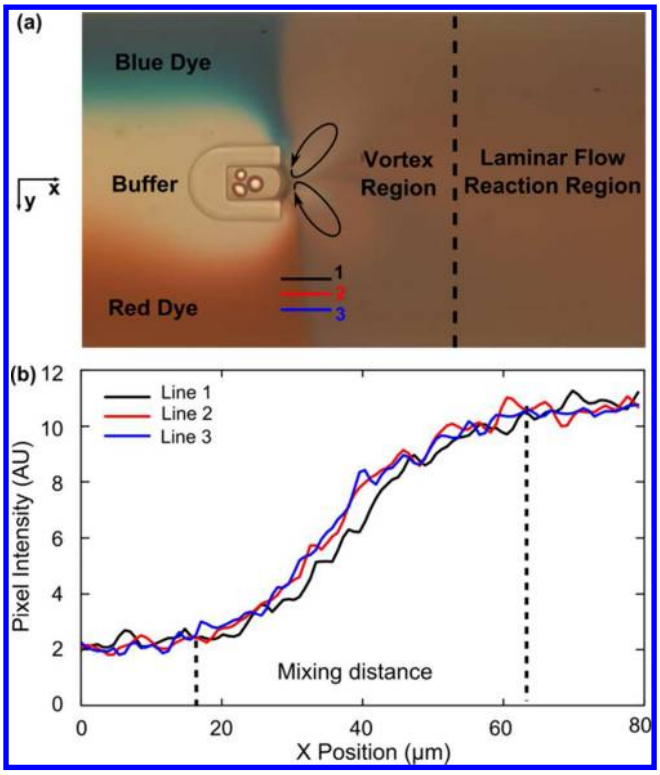

Figure 2. (a) Mixing caused by an oscillating bubble surface. Water and dyes were used to demonstrate the mixing effect of enzyme and substrate. (b) Line analysis to calculate mixing time.

activates, three distinct regions of streamlines exist in the channel by using fluorescent polystyrene particles with a diameter of 1 μm (Figure S1 in the Supporting Information). The first region, in which the streamlines are parallel indicating laminar flow, occurs before the fluid reaches the bubble. The second region is the vortex region in which rapid mixing takes place. The vortex flow pattern is similar to the streaming pattern near a bubble, driven by bulk acoustic waves.[46−48] Significantly downstream of the bubble exists the third region where the effect of the bubble oscillation is negligible and the streamlines are again parallel. All concentration measurements were made in the third region.

In order for the substrate and enzyme to be fully mixed before significant amount of product is generated, the mixing time must be significantly shorter than the reaction time. The average mixing time (t_{avg}) could be estimated by

$$t_{avg} = \frac{d_{mix}}{v_{avg}} \quad (1)$$

where d_{mix} was the average mixing distance and v_{avg} was the average velocity of flow in the channel. The average mixing distance d_{mix} was characterized using a gray value plot (Figure 2a, lines 1−3) in the region from unmixed to mixed. The distance in the x direction of the sloped part of the gray value curve (Figure 2b) was the mixing distance. Data from three separate locations (lines 1−3) were plotted to get the average mixing distance (around 45 μm). The average velocity of flow in the channel (v_{avg}) could be calculated by flow rate and channel dimension. Under the experimental conditions (total flow rate, 1.1 μL/min), t_{avg} was about 89 ms. Such a mixing time is significantly shorter than the enzymatic reaction time (several seconds). Therefore, we could assume that the reagents were fully mixed before the reaction started. Moreover, our acoustic bubble based mixer could still achieve excellent mixing when the total flow rate increased; at a flow rate of 10 μL/min, the mixing time was even shorter (~10 ms).

Calibration Curve. A standard curve of product samples with different concentrations was generated to obtain the relationship between the concentration and fluorescent intensity of product. Standard product material with a concentration of 2 μM was mixed with buffer in different ratios to form a series of concentrations. After mixing by the oscillating bubble, the concentrations were 0.0, 0.2, 0.4, 0.6, 0.8, 1.0, 1.2, 1.4, 1.6, 1.8, and 2.0 μM. After mixing, the fluorescent intensity was detected by a CCD camera. All experimental conditions for fluorescence detection were the same as in our enzymatic reaction experiments. Figure 3a shows a single image

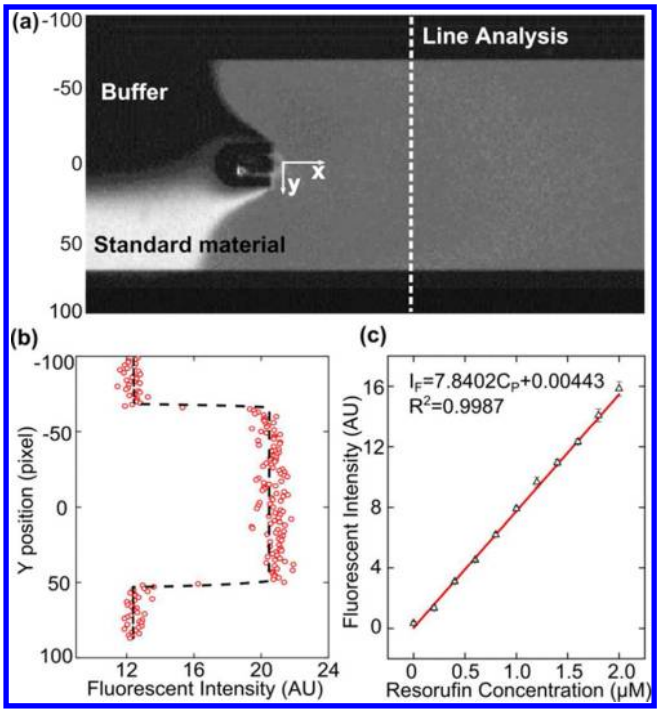

Figure 3. (a) Optical image recorded during the calibration experiment. (b) Fluorescent intensity at the detection line. The difference between liquid in the channel and background was used as effective fluorescent intensity. (c) The standard curve of product fluorescent intensity.

recorded during the calibration experiment. In this picture, the flow rate ratio between standard material and buffer was 1:1. The fluorescent intensity along the channel-width direction (y direction) is plotted in Figure 3b. The difference between the fluorescence of the liquid and the dark background was used as the effective fluorescent intensity. The entire calibration experiment was repeated three times to produce the calibration curve shown in Figure 3c. The points represent the mean for each test and the error bar represents the standard deviation. A least-squares fit of the data was performed to generate the relation equation:

$$I_F = 7.8402C_P + 0.00443 \quad (2)$$

Here, I_F is fluorescent intensity (arbitrary unit) and C_P is the concentration of product (μM). This equation was used to correlate product concentration with fluorescent intensity in the following sections.

dx.doi.org/10.1021/ac301590y | Anal. Chem. 2012, 84, 7495−7501

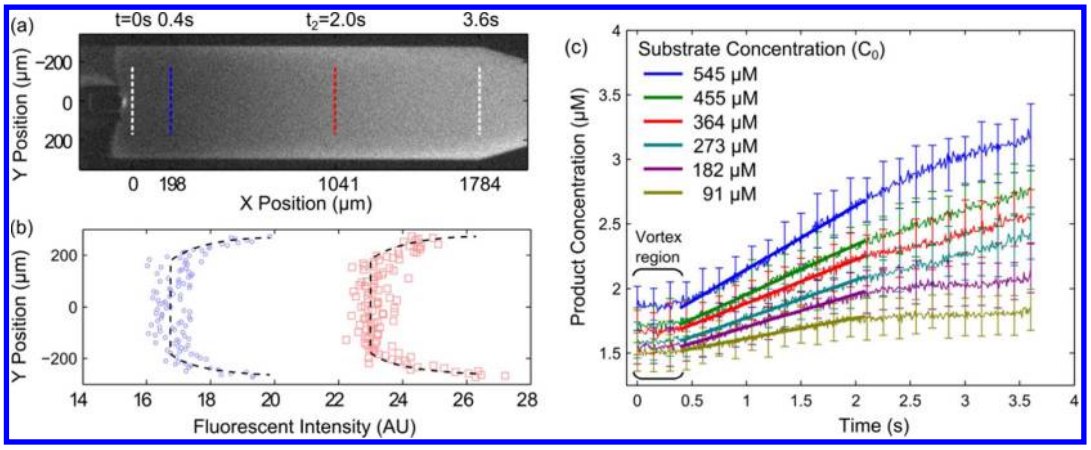

Figure 4. (a) Enzymatic reaction carried out in the channel. The fluorescent intensity was detected in the channel with equal distance intervals. (b) The fluorescent intensity at the starting point of reaction (circle) and the point after a certain reaction time (square). The fluorescent intensity at the middle of the curves was used as effective fluorescent intensity in Figure 4c. (c) Initial reaction rate (v_0) curve with substrate concentration ranging from 91 μM to 545 μM. The concentration of enzyme was set as 5 mg/L.

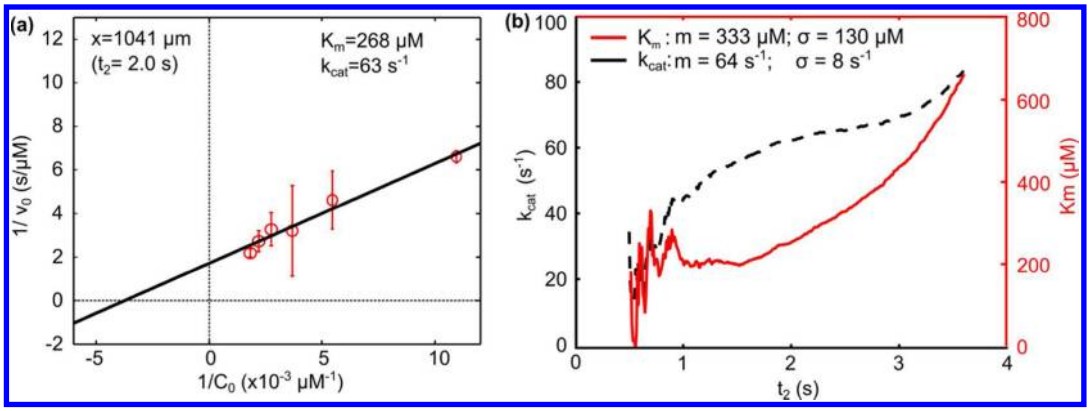

Figure 5. (a) Lineweaver–Burk plot to characterize K_m and k_{cat} on single initial reaction time. (b) K_m and k_{cat} analysis under different reaction times.

Enzymatic Reaction Rate. In our device, fast mixing allows us to measure v_0 in a short time (subsecond range). For this enzymatic reaction, the enzyme concentration was 5 mg/L, which is sufficient to cause a detectable fluorescent change in the 1 s range. Accordingly, we chose a substrate concentration series ranging from 91 to 545 μM with an interval of 91 μM. The concentration series was generated by using different flow rate ratios between substrate stock solution (1 mM) and reaction buffer (Figure S7 in the Supporting Information).

Total flow rate is an important factor, which decides the reaction time in the channel. When the flow rate is larger, the residence time is shorter, which means that the enzyme has a shorter time to generate product. As a result, the product concentration is smaller. On the basis of the preliminary research, the total flow rate was always held at 1.1 μL/min (enzyme, 0.5 μL/min; substrate, 0.6–0.0 μL/min; buffer, 0.0–0.6 μL/min). The average residence time in the channel was about 4 s, which is long enough to produce an obvious change in fluorescent intensity along the length of the channel. The velocity profile in the channel was another key factor. Because the channel width (570 μm) was much larger than the channel depth (65 μm), the velocity across the width of channel was almost uniform except at the edges, and the velocity across the depth of channel was parabolic causing concentration changes near the edges.[49,50] As a simplification, we neglected the parabolic velocity profile in the depth direction and used the average velocity to calculate the reaction time. We established a mathematic model (details in the Supporting Information) to theoretically predict the difference in the product generated between plug flow and laminar flow to be less than 5%. The Peclet number is still much larger than one at the flow rates we used, so the axial dispersion effect can also be safely neglected.

The images taken by the CCD camera were imported to a Matlab program for data analysis. Figure 4a shows a single experimental image demonstrating how the fluorescent intensity was analyzed in the experiment. Analysis of the gray scale value across the channel width was used to detect fluorescent intensity. The gray scale plots of two representative results at different X positions (blue and red line in Figure 4a) are shown in Figure 4b. These plots are the average values over 10 pixels in the X-direction. It can be seen that the upstream data (blue circles) have less fluorescence when compared to the downstream data (red squares). As the reagents move down the channel more product is generated. At the edge of the channel the velocity is lower because of the laminar flow profile in the channel, so the intensity, and likewise concentration of product, increases more rapidly. Therefore, we only used the data at the center of the channel (between $Y = -200$ and 200 μm) to calculate the fluorescence value at each X position. The mean and standard deviation of this fluorescent intensity in Figure 4b were correlated to product concentration by the calibration curve (Figure 3c) and displayed as one data point in Figure 4c. Also the X distance was correlated with reaction time by channel dimension and flow rate. The reaction time was

dx.doi.org/10.1021/ac301590y | Anal. Chem. 2012, 84, 7495–7501

calculated by dividing the X distance by plug flow velocity (496 μm/s). The fluorescence at each X position starting at the surface of the bubble (x = 0 μm, t = 0 s) to the very end of the straight channel (x = 1784 μm, t = 3.6 s) was analyzed with a resolution of 1 pixel (Δx = 4.96 μm; Δt = 0.01 s) and plotted as a function of product concentration versus reaction time in Figure 4c. This was repeated for each substrate concentration (C_0) between 91 and 545 μM (Figure S4 in the Supporting Information). At the beginning of each set of data, the trend was flat because the reaction had yet to start. The baseline fluorescence is not exactly the same for each initial concentration because the substrate sample contains some fluorescent product due to degradation.

Once the reaction starts, the fluorescence increases linearly in accordance with M−M kinetics. The linear increase part began at point x = 198 μm (t = 0.4 s), and this point was shown in Figure 4a by the blue line. From this point, a least-squares, linear fit can be used to find the reaction rate (v_0) because this initial part of the enzyme reaction has a linear trend and the slope of the linear fit is v_0. Using the calculated value of v_0, the reaction constants K_m and k_{cat} can be calculated via the L−B plot analysis described in the next section. Since our system records information during the initial reaction at high resolution, we could conveniently choose different initial reaction times to analyze. The reaction time is defined from the start of the linear region (t = 0.4 s, blue line in Figure 4a) to some later time, which we denote as t_2. As an example, we analyze the system using t_2 = 2.0 s (red line in Figure 4a). This is the value of t_2 used to generate the linear fits shown in Figure 4c. The calculated v_0 values are plotted in Figure 5a and used to determine K_m and k_{cat} as described in the next section. This process is repeated for values of t_2 from 0.5 to 3.6 s with a resolution of 0.01 s.

Lineweaver−Burk Plot. The L−B plot derived from the M−M mechanism is described by[7]

$$\frac{1}{v_0} = \frac{K_m}{V_{max}}\frac{1}{C_0} + \frac{1}{V_{max}} \quad (3)$$

where $1/v_0$ has a linear relationship with $1/C_0$, the slope is K_m/V_{max}, the y-intercept is $1/V_{max}$ (where V_{max} is the maximum reaction rate), and the x-intercept is $-1/K_m$. From the relationship in eq 3, K_m and k_{cat} can be calculated. Continuing the example where t_2 = 2 s (between the blue and red lines in Figure 4a), Figure 5a was generated from the values of v_0 determined from the linear fits shown in Figure 4c. The enzymatic reaction was repeated three times and the mean and standard deviation of v_0 were calculated. The reciprocal of v_0 was plotted against the reciprocal of C_0 in Figure 5a where the points represent the mean and the error bars represent the standard deviation of v_0. A least-squares linear fit of the mean values was calculated, and the slope of the fitting line was K_m/V_{max}, and the y-intercept was $1/V_{max}$. K_m for this example at t_2 = 2 s was 268 μM, and the value of k_{cat} can be calculated by[13]

$$V_{max} = k_{cat}[E] \quad (4)$$

where [E] is the concentration of the enzyme. Thus for t_2 = 2 s, the value of k_{cat} was 63 s^{-1}.

To fully characterize the reaction constants for different initial reaction times, we repeated this entire analysis process for different values of t_2 between 0.5 and 3.6 s with a resolution of 0.01 s. The results were shown in Figure 5b. Theoretically, K_m and k_{cat} should be kept constant. However, because of the slight decrease in v_0 as t_2 increases and the amplified error due to the two reciprocals in the linear regression (Figure 5a), K_m and k_{cat} are not constant with respect to t_2. To produce an average K_m and k_{cat} to compare with other published data, we calculated the mean and standard deviation of K_m and k_{cat} over a range of t_2. We ignored the data over the range t_2 = 0.5−1 s, because in this period the number of data points was low, causing erratic linear fits to produce v_0, thus K_m and k_{cat} fluctuate during this period. From t_2 = 1−3.6 s, K_m had a mean of 333 μM and a standard deviation of 130 μM, and k_{cat} had a mean of 64 s^{-1} and a standard deviation of 8 s^{-1}. This data should be an accurate, comprehensive description of our device because it considers the error from both parallel experiments (as represented by error bars in Figure 5a) and different reaction times (as represented by the presented standard deviations of K_m and k_{cat}).

We listed our results and the data from previously reported work in Table 1. To compare the difference between our results and published data, a two-tailed t test was conducted. We assumed the null hypothesis that there was no significant difference between these three independent studies. When it was unknown, the number of tests performed was assumed to be three for the t test. The P-values calculated for each comparison are given in Table 2. Using a significance level of 0.1, the t test indicates that we cannot reject the null hypothesis in comparing K_m between group 1 and 3, 2 and 3 and k_{cat} between group 2 and 3, which states that these results have no significant difference. On the other hand, there is difference between groups 2 and 3 in comparing k_{cat}.

Table 1. Comparing Results of K_m and k_{cat}

no.	K_m (μM)	k_{cat} (/s)	author
1	550 ± 200	70 ± 30	Hadd[35]
2	335 ± 65	39 ± 5	Jambovane[51]
3	333 ± 130	64 ± 8	this work

Table 2. P-Value from t-Test for K_m and k_{cat}

compare group no.	P for K_m	P for k_{cat}
1 and 3	0.214	0.792
2 and 3	0.930	0.058

Overall, our results compared reasonably well with the reported data from Hadd[35] et al. and Jambovane[51] et al. There are several reasons for the discrepancies between our results and published data. First, although the enzyme and substrate were the same in each work, the enzyme activity might vary in different batches and the properties of reaction buffer might not be consistent. The enzyme activity is dependent on its environment and these small differences could change enzyme activity. Second, the flow model we used was an ideal plug flow, meaning each portion of the fluid has the same residence time; however, the flow condition in the experiments was more complicated, including a parabolic velocity profile and slight flow instabilities from the syringe pumps and channel inlets. Third, the lack of fast mixing in the previous works affected the final results. Fourth, factors in the data analysis method and sample processing such as line analysis interval affect the results. In our case, the values of K_m and k_{cat} were dependent on the reaction time. We have shown this trend in Figure 5b. Jambovane also mentioned that using alternate methods for

dx.doi.org/10.1021/ac301590y | Anal. Chem. 2012, 84, 7495−7501

data analysis could cause variation of as much as 13% for K_m and 24% for k_{cat}.[51]

CONCLUSIONS

In summary, we performed a single-shot enzymatic reaction using a bubble-based micromixer. This device could simply and quickly characterize enzymatic reaction constants. Each data set was collected in 1 s. Fast mixing of enzyme and substrate in under 100 ms was achieved by an acoustically driven bubble anchored in a horseshoe structure. Our design overcame the low mixing speed and efficiency of earlier microfluidic designs. The "single shot" detection system does not require preparation of additional samples for each parallel experiment, as adjusting flow rates conveniently alters the concentration ratio. The continuous flow reaction allowed all product concentration information in initial enzymatic reaction to be recorded with high resolution. The β-galactosidase-catalyzed hydrolysis of resorufin β-D-galactopyranoside was tested as a model system and K_m and k_{cat} in this reaction were measured to be 333 μM, with a standard deviation of 130 μM, and 64 s^{-1} with a standard deviation of 8 s^{-1}, respectively. These values are in fair agreement with published results. Our approach reduced mixing time into the milliseconds range, significantly increasing the efficiency in characterizing enzymatic reaction constants. It represents the ability to study kinetics of high-speed enzymatic reactions with small amounts of enzymes, substrates, or inhibitors.

ASSOCIATED CONTENT

Supporting Information

Additional information and figures. This material is available free of charge via the Internet at http://pubs.acs.org.

AUTHOR INFORMATION

Corresponding Author

*Phone: 814-863-4209. Fax: 814-865-9974. E-mail: junhuang@psu.edu.

Notes

The authors declare no competing financial interest.

ACKNOWLEDGMENTS

The authors thank Matt Jaffe and Jason Scott for helpful discussions. This research was supported by National Institutes of Health (Director's New Innovator Award, Grant 1DP2OD007209-01), National Science Foundation, U.S. Department of Agriculture (USDA/NRI), and the Penn State Center for Nanoscale Science (MRSEC). Components of this work were conducted at the Penn State node of the NSF-funded National Nanotechnology Infrastructure Network.

REFERENCES

(1) Roach, P. *Nature* **2011**, *478*, 463−464.
(2) Wallman, L.; Åkesson, E.; Ceric, D.; Andersson, P.; Day, K.; Hovatta, O.; Falci, S.; Laurell, T.; Sundström, E. *Lab Chip* **2011**, *11*, 3241−3248.
(3) Prendergast, G. C. *Nature* **2011**, *478*, 192−194.
(4) Panicco, P; Dodhia, V. R.; Fantuzzi, A.; Gilardi, G. *Anal. Chem.* **2011**, *83* (6), 2179−2186.
(5) Morton, R. A. *Nature* **1962**, *193*, 15−17.
(6) Jokerst, J. C.; Adkins, J. A.; Bisha, B.; Mentele, M. M.; Goodridge, L. D.; Henry, C. S. *Anal. Chem.* **2012**, *84* (6), 2900−2907.
(7) Yoshikuni, Y.; Ferrin, T. E.; Keasling, J. D. *Nature* **2006**, *440*, 1078−1082.
(8) Raz, S. R.; Liu, H.; Norde, W.; Bremer, M. G. E. G. *Anal. Chem.* **2010**, *82* (20), 8485−8491.
(9) Mazutis, L.; Baret, J.; Treacy, P.; Skhiri, Y.; Araghi, A.; Ryckelynck, M.; Taly, V.; Griffiths, A. *Lab Chip* **2009**, *9*, 2902−2908.
(10) Copeland, R. *Enzymes: A Practical Introduction to Structure, Mechanism, and Data Analysis*; Wiley-VCH: New York, 2000.
(11) Copeland, R. *Evaluation of Enzyme Inhibitors in Drug Discovery: A Guide for Medicinal Chemists and Pharmacologists*; John Wiley and Sons: Hoboken, NJ, 2005.
(12) Menten, L.; Michaelis, M. I. *Biochemistry* **1913**, *49*, 333−369.
(13) Lehninger, A. L.; Nelson, D. L.; Cox, M. M. *Lehninger Principles of Biochemistry*; W.H. Freeman: New York, 2005.
(14) Lineweaver, H.; Burk, D. *J. Am. Chem. Soc.* **1934**, *56*, 658−666.
(15) Whitesides, G. M. *Nature* **2006**, *442*, 368−373.
(16) Liu, S.; Li, Q.; Shao, Y. *Chem. Soc. Rev.* **2011**, *40*, 2236−2253.
(17) Liu, K. J.; Brock, M. V.; Shih, I. M.; Wang, T. H. *J. Am. Chem. Soc.* **2010**, *132* (16), 5793−5798.
(18) Mellors, J. S.; Gorbounov, V.; Ramsey, R. S.; Ramsey, J. M. *Anal. Chem.* **2008**, *80*, 6881−6887.
(19) Keyes, J.; Junkin, M.; Cappello, J.; Wu, X.; Wong, P. K. *Appl. Phys. Lett.* **2008**, *93*, 023120.
(20) Hennig, M.; Neumann, J.; Wixforth, A.; Rädler, J.; Schneider, M. *Lab Chip* **2009**, *9*, 3050−3053.
(21) Hong, J. W.; Studer, V.; Hang, G.; Anderson, N. F.; Quake, S. R. *Nat. Biotechnol.* **2004**, *22*, 435−439.
(22) Agarwal, G.; Livermore, C. *Lab Chip* **2011**, *11*, 2204−2211.
(23) Mao, X.; Waldeisena, J. R.; Huang, T. J. *Lab Chip* **2007**, *7*, 1260−1262.
(24) Shi, J.; Yazdi, S.; Lin, S.-C. S.; Ding, X.; Chiang, I.; Sharpd, K.; Huang, T. J. *Lab Chip* **2011**, *11*, 2319−2324.
(25) Lapsley, M. I.; Chiang, I.; Zheng, Y. B.; Ding, X.; Mao, X.; Huang, T. J. *Lab Chip* **2011**, *11*, 1795−1800.
(26) Lenshof, A.; Laurell, T. *Chem. Soc. Rev.* **2010**, *39*, 1203−1217.
(27) Shi, J.; Mao, X.; Ahmed, D.; Colletti, A.; Huang, T. J. *Lab Chip* **2008**, *8*, 221−223.
(28) Miller, E. M.; Wheeler, A. R. *Anal. Chem.* **2008**, *80*, 1614−1619.
(29) Kang, J. H.; Park, J. *Sens. Actuators, B* **2005**, *107*, 980−985.
(30) Liu, A.; Zhou, T.; He, F.; Xu, J.; Lu, Y.; Chen, H.; Xia, X. *Lab Chip* **2006**, *6*, 811−818.
(31) Wang, C.; Li, S.; Wu, Z.; Xu, J.; Chen, H.; Xia, X. *Lab Chip* **2010**, *10*, 639−646.
(32) Weis, D. D.; Nardozzi, J. D. *Anal. Chem.* **2005**, *77*, 2558−2563.
(33) Song, H.; Ismagilov, R. F. *J. Am. Chem. Soc.* **2003**, *125*, 14613−14619.
(34) Song, H.; Chen, D. L.; Ismagilov, R. F. *Angew. Chem., Int. Ed.* **2006**, *45*, 7336−7356.
(35) Hadd, A. G.; Raymond, D. E.; Halliwell, J. W.; Jacobson, S. C.; Ramsey, J. M. *Anal. Chem.* **1997**, *69*, 3407−3412.
(36) Seong, G. H.; Heo, J.; Crooks, R. M. *Anal. Chem.* **2003**, *75*, 3161−3167.
(37) Ristenpart, W. D.; Wan, J.; Stone, H. A. *Anal. Chem.* **2008**, *80*, 3270−3276.
(38) Seong, G. H.; Crooks, R. M. *J. Am. Chem. Soc.* **2002**, *124*, 13360−13361.
(39) Clausell-Tormos, J.; Griffiths, A. D.; Merten, C. A. *Lab Chip* **2010**, *10*, 1302−1307.
(40) Bui, M. P.; Li, C. A.; Han, K. N.; Choo, J.; Lee, E. K.; Seong, G. H. *Anal. Chem.* **2011**, *83*, 1603−1608.
(41) Srisa-Art, M.; Dyson, E. C.; deMello, A. J.; Edel, J. B. *Anal. Chem.* **2008**, *80*, 7063−7067.
(42) Srinivasan, V.; Pamula, V. K.; Fair, R. B. *Anal. Chim. Acta* **2004**, *507*, 145−150.
(43) Ahmed, D.; Mao, X.; Shi, J.; Juluri, B. K.; Huang, T. J. *Lab Chip* **2009**, *9*, 2738−2741.
(44) Ahmed, D.; Mao, X.; Juluri, B. K.; Huang, T. J. *Microfluid. Nanofluid.* **2009**, *7*, 727−731.
(45) Xia, Y.; Whitesides, G. M. *Annu. Rev. Mater. Sci.* **1998**, *28*, 153−184.

(46) Tho, P.; Manasseh, R.; Ooi, A. *J. Fluid Mech.* **2007**, *576*, 191−233.
(47) Collis, J.; Manasseh, R.; Liovic, P.; Tho, P.; Ooi, A.; Petkovic-Duran, K.; Zhu, Y. *Ultrasonics* **2010**, *50*, 273−279.
(48) Riley, N. *Theor. Comput. Fluid Dyn.* **1998**, *10*, 349−356.
(49) Ismagilov, R. F.; Stroock, A. D.; Kenis, P. J. A.; Whitesides, G.; Stone, H. A. *Appl. Phys. Lett.* **2000**, *76*, 2376.
(50) Salmon, J. B.; Ajdari, A. J. *Appl. Phys.* **2007**, *101*, 074902.
(51) Jambovane, S.; Duin, E.; Kim, S.; Hong, J. W. *Anal. Chem.* **2009**, *81* (9), 3239−3245.